Hydrothermal Synthesis, Structure and Magnetic Properties of a One-Dimensional Iron Arsenate, $^1_\infty[NH_3(CH_2)_2NH(CH_2)_2NH_3][Fe_2F_4(HAsO_4)_2]$

Sandip Chakrabarti,[a] Swapan K. Pati,[b] Mark A. Green,[c] and Srinivasan Natarajan*[a]

Keywords: Iron arsenate / Antiferromagnetism / Hydrothermal reactions / Iron / Magnetic properties

A novel one-dimensional iron arsenate, $^1_\infty[NH_3(CH_2)_2NH(CH_2)_2NH_3][Fe_2F_4(HAsO_4)_2]$, built up exclusively from SBU-4 units (two octahedral units sharing an edge and connected through two tetrahedra) with Fe^{3+} ions in the high-spin state has been synthesized by hydrothermal methods. Structure elucidation reveals that the compound is a two-leg ladder with very weak antiferromagnetic exchanges along the chains. The magnetic susceptibility data show activated behaviour at T = 14 K, suggesting a finite spin gap between the nonmagnetic ground state and the excited triplet state. We have estimated the exchange parameters theoretically based on the S = 5/2 Majumdar–Ghosh model with frustrations and dimerisations. Although the magnetic gap is quite small, this is the first example, to the best of our knowledge, where the rungs with two S = 5/2 spins form strong singlet dimers.

(© Wiley-VCH Verlag GmbH & Co. KGaA, 69451 Weinheim, Germany, 2004)

Introduction

In recent years, one-dimensional and quasi-one-dimensional systems have received considerable attention. Due to large quantum fluctuations, low-dimensional systems often show unusual properties such as a gap between a singlet ground state and a magnetic excited state; this leads to exponentially vanishing magnetic susceptibility at low temperature. Many low-dimensional systems have been realised experimentally, of which the Haldane gap spin-1 system is a good example.[1−3] Other examples include the spin-ladder systems in which a small number of chains interact with each other.[4,5] It has been observed that if each rung of the ladder contains an odd number of spin-1/2 sites, then the system effectively behaves like a spin-1/2 chain with a gapless low-energy spectrum. Such behaviour has been observed in $Sr_2Cu_3O_5$.[6] Conversely, ladders with an even number of spin-1/2 sites in the rung behave like an integer spin chain with a finite spin gap to the lowest excited spin state [for example, $SrCu_2O_3$,[7] $(VO)_2P_2O_7$,[8] $Cu_2(C_5H_{12}N_2)_2Cl_4$ [9]]. Another interesting observation in a quasi-one-dimensional spin system, $CuGeO_3$, is that it spontaneously dimerises below the spin-Peierls transition temperature leading to opening up of a spin gap.[10]

We have been interested in the intricate relationship between structure, dimensionality and magnetism. As part of a research program aiming to produce new compounds based on iron, a new iron arsenate, $^1_\infty[NH_3(CH_2)_2NH(CH_2)_2NH_3][Fe_2F_4(HAsO_4)_2]$ (**I**), possessing a one-dimensional structure was synthesized. Although the syntheses and structures of a large number of metal phosphates with open-framework structures have been reported in the literature,[11] research on metal arsenates is just beginning to emerge.[12−16] In many of the metal phosphates, the use of fluorine in the synthesis mixture appears to give rise to a variety of novel structures, especially in iron phosphates.[17] The concept of secondary building units has evolved to describe complex crystal structures based on tetrahedral connectivity.[18] During the last few years, this has been expanded to include nontetrahedral connectivity as well.[19] In the case of octahedral-tetrahedral structures, such as those present in iron phosphates and arsenates, the common structural features prompted Ferey to propose a set of secondary building units (SBUs) to describe and understand such structures.[20−22] The simplest of the SBUs is the one containing two octahedral and tetrahedral units (SBU-4), wherein the octahedral units share edges/corners and are connected through the tetrahedra. Compound **I**, described here, is the first one-dimensional structure built up exclusively from SBU-4 building units.

The two-leg ladder $^1_\infty[NH_3(CH_2)_2NH(CH_2)_2NH_3][Fe_2F_4(HAsO_4)_2]$ (**I**) consists of high-spin Fe^{3+} (S = 5/2) ions. Due to strong exchange interactions between the rung

[a] Framework Solids Laboratory, Chemistry and Physics of Materials Unit, Jawaharlal Nehru Centre for Advanced Scientific Research,
Jakkur P. O., Bangalore 560064, India
Fax: (internat.) + 91-80-2362-2766
E-mail: raj@jncasr.ac.in
[b] Theoretical Sciences Unit, Jawaharlal Nehru Centre for Advanced Scientific Research,
Jakkur P. O., Bangalore 560 064, India
[c] The Davy-Faraday Research Laboratory, The Royal Institution of Great Britain,
21 Albemarle Street, London, W2S 4BS, UK

 © 2004 Wiley-VCH Verlag GmbH & Co. KGaA, Weinheim DOI: 10.1002/ejic.200400127

spins, each rung can be considered as a singlet spin dimer. The magnetic susceptibility measurements show that the system has a spin gap of about 10 K. The theoretical fit to the experimental data suggests that the system is a weakly linked rung dimer. We have also measured magnetisation as a function of magnetic field at two different temperatures. At low field strength, both of the magnetisation curves follow unit-cell-polarised Brillouin functions (each unit cell contains two $S = 5/2$).

Results and Discussion

The asymmetric unit of **I** contains two crystallographically unique Fe and As atoms. Of these, Fe(1) and As(1), and Fe(2) and As(2) are connected together, giving rise to two independent one-dimensional ladders. Both the Fe atoms, Fe(1) and Fe(2), are octahedrally coordinated by three O and three F atoms with Fe−O/F bond lengths in the range 1.874(3)−2.064(3) Å (average 1.9852 Å). Each iron atom is linked to three arsenic atoms through three Fe−O−As bonds (average angle 127.5°), has two Fe−F−Fe bonds (average angle 101.43°) and possesses a terminal Fe−F bond. Each As atom also has three As−O−Fe bonds and one terminal As−O bond. The As atom is tetrahedrally coordinated by oxygen atoms with an average As−O distance of 1. 6832 Å and an O−As−O bond angle of 109.4°. The terminal As−O bonds, for both As(1) and As(2), are As−OH bonds; this agrees well with the proton position found next to the oxygen atoms in the difference Fourier map. The Brown−Altermatt formalism[23] for the bond length/bond valence relationship for Fe−O, Fe−F and As−O was used to calculate bond-order sums for the cations and anions (Table 3). The calculated bond-order sums for both cations and anions are in agreement with the formal oxidation states of +3, +5 and −2 for Fe, As and O atoms, respectively (Table 3).

The structure of **I** consists of FeO_3F_3 octahedral and $HAsO_4$ tetrahedral building units connected through their vertices. Thus, the connectivity between $Fe(1)O_3F_3$ and $As(1)O_3(OH)$, and $Fe(2)O_3F_3$ and $As(2)O_3(OH)$ gives rise to two distinctand independent one-dimensional structure units (Figure 1). The FeF_3O_3 octahedra are connected together through two Fe−F−Fe bridges forming edge-shared dimers. The $Fe_2F_4O_6$ dimers are linked through $AsO_3(OH)$ tetrahedra completing the basic building unit, which resembles the secondary building unit, SBU-4, enumerated by Ferey.[20−22] The SBU-4 units are joined together to give rise to the one-dimensional ladder structure (Figure 1). The charge-compensating doubly protonated diethylenetriamine (DETA) molecules are located between the ladders and interact through N−H···O and N−H···F hydrogen bonds. The view of the ladders and the arrangement of the SBU-4 units along the *c* axis are shown in Figure 2. The presence of terminal fluoride, along with OH groups, gives rise to a number of hydrogen-bond interactions involving the amine. Important hydrogen-bond interactions are listed in Table 1.

The presence of Fe_2F_2 dimers in **I**, and strong intrachain and weak interchain interactions between the SBU-4 units

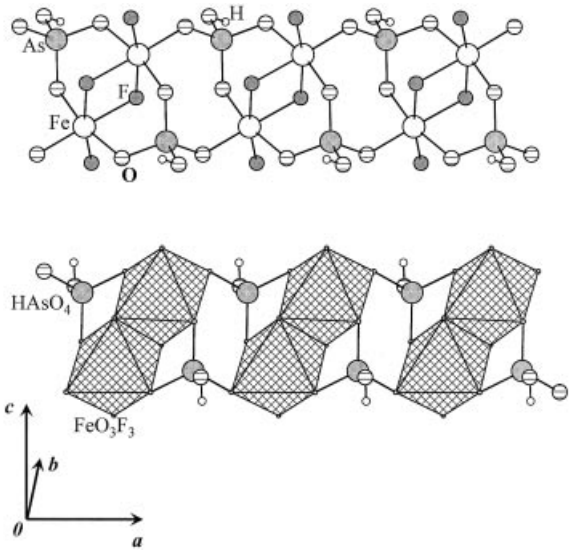

Figure 1. Structure of **I** showing the arrangement of the ladders; note that the SBU-4 units are connected through a four-membered ring; amine molecules are not shown for clarity

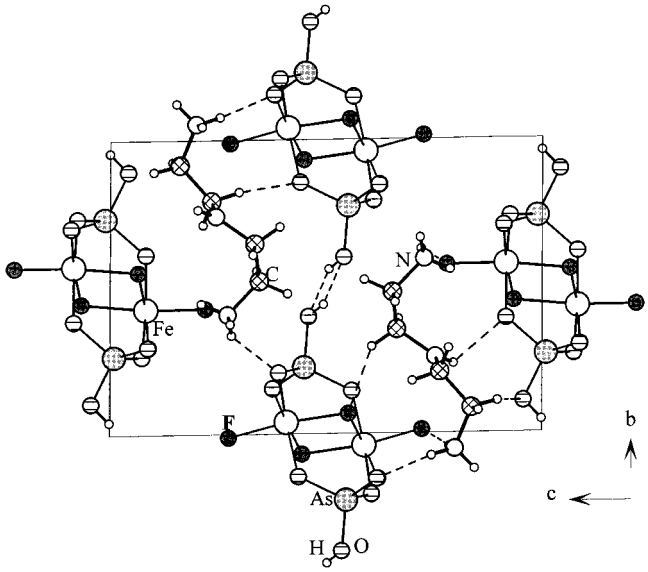

Figure 2. Structure of **I** viewed down the ladder axis; dotted lines represent possible hydrogen-bond interactions

prompted us to evaluate the magnetic properties of **I**. The magnetic characterization of **I** was carried out using a SQUID magnetometer in the temperature range 5−300 K. The temperature dependence of the magnetic susceptibility (χ) of **I** is shown in Figure 3. The special feature to be noticed is the activated behaviour at $T \approx 14$ K, below which the susceptibility (χ) drops exponentially to zero. This activated behaviour corresponds to a finite spin gap in the material. For low-dimensional spin-gap systems, considering the magnon excitations approximately, Troyer et al. have derived a general expression for χ: $\chi = (1/K_BT)z(K_BT)/[1 + 3z(K_BT)]$, with $z(K_BT) = 1/\pi \int \exp(-E_K/K_BT)dK$, where E_K is the nondegenerate triplet magnon dispersion.[24] For low temperature, the above expression can be approximated as

 © 2004 Wiley-VCH Verlag GmbH & Co. KGaA, Weinheim

Table 1. Important hydrogen-bond interactions in $^1_\infty[NH_3(CH_2)_2NH(CH_2)_2NH_3][Fe_2F_4(HAsO_4)_2]$ (**I**); symmetry operations used to generate equivalent atoms: #1: $1-x, y, 1+z$; #2: $2-x, 1-y, 3-z$; #3: $x, 1+y, 1+z$; #4: $x, 1+y, z$; #5: $1-x, 1-y, 3-z$

D−H···A	D−H [Å]	H···A [Å]	D···A [Å]	D−H···A [°]
N(1)−H(1)···O(6)	0.89	2.05	2.801(6)	141
N(1)−H(2)···F(11)#1	0.89	2.44	3.294(6)	161
N(2)−H(8)···O(1)#2	0.86	2.62	3.253(7)	144
N(3)−H(13)···O(3)#3	0.89	2.22	3.015(7)	148
N(3)−H(14)···O(8)#4	0.89	2.01	2.886(7)	170
N(3)−H(15)···F(10)#4	0.89	1.94	2.803(7)	162
O(7)−H(30)···O(7)[a]#2	0.82	1.78	2.524(6)	151
C(2)−H(7)···F(9)#4	0.97	2.25	3.092(7)	144
C(3)−H(10)···O(5)#2	0.97	2.29	3.238(8)	165
C(4)−H(11)···O(1)#5	0.97	2.43	3.327(8)	154

[a] Interchain interaction.

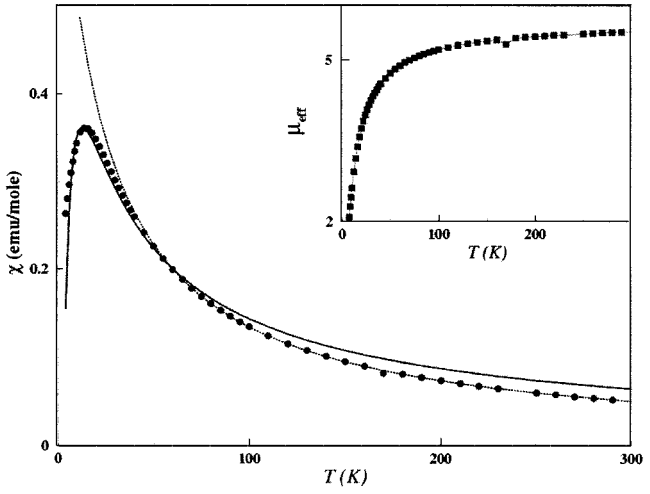

Figure 3. χ [emu/mol] vs. T plot at 100 Gauss; the solid line is the exponential fit at low temperature mentioned in the text; the dotted line is the Curie−Weiss law fit for χ at high temperature; the inset shows the effective magnetic moment μ_{eff} as a function of T

$\chi_{low\text{-}T} = A\cdot\exp(-\Delta/K_BT)/(K_BT)^{\zeta}$. This formulation can be applied for any half-integer spin with parabolic triplet magnon dispersion at low temperature.[25] Note that, at the dimer limit, $\Delta = 1$ and the exponent ζ becomes 1. However, for a gapped spin-1/2 extended lattice, it is shown that $\zeta = 1/2$. Clearly, this exponent relates the transition from a dimer limit to the extended system. By fitting the above form of $\chi_{low\text{-}T}$ with the experimental data, we find that the best fit is obtained with $A = 6$, $\Delta = 10.3$ K and $\zeta = 0.78$. The fit is shown as a solid line in Figure 3. At high temperature, the value of χ saturates to the paramagnetic value for two $S = 5/2$ spins. The high-temperature susceptibility, $\chi_{high\text{-}T}$, fits very well down to $T = 60$ K with a Curie−Weiss form $\chi_{cw} = C/(T-\Theta)$, with $C = 16.39$ and $\Theta = -22$ K (dotted line in Figure 3). The inset shows the effective magnetic moment μ_{eff} as a function of temperature. The room-temperature μ_{eff} per Fe is approximately equal to 5.5 μ_B, which steadily decreases to 1.45 μ_B at 5 K, indicating strong antiferromagnetic behaviour (see inset, Figure 3). This room-temperature value of μ_{eff} compares fairly well with the spin-only moment for high-spin Fe^{3+}.

The maximum and the subsequent decrease of χ with an increase in T correspond to short-range antiferromagnetic exchange interactions in the system. A careful investigation of the structure reveals that there are three different superexchange pathways as shown below in Scheme 1. All the superexchange angles between the corresponding pair of localised Fe^{3+} ions through the intervening atoms suggest that all three exchanges are antiferromagnetic, making the system highly frustrated. In addition, J_1 exchanges in the rung (Fe dimers) are through two fluorine atoms, while J_2 and J_3 are through $HAsO_4$ tetrahedral links. This clearly shows that the intradimer exchange interactions are much stronger than the interdimer exchanges. Although we specify two different exchanges between the rungs, they are similar in magnitude and are quite small relative to J_1.

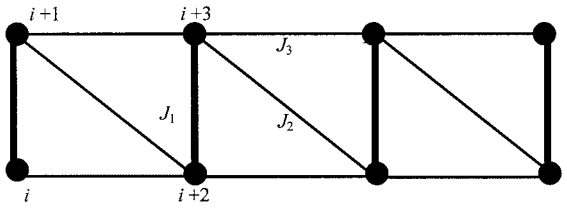

Scheme 1

If we neglect J_3, the system is a $S = 5/2$ J-alternating one-dimensional chain with exchange values J_1 and J_2 respectively. If $J_1 = J_2$, the system is an isotropic half-integer spin chain, which is gapless. Defining $\alpha = J_1/J_2$, for small J_2, the spin gap increases as $\alpha^{2/3}$ with increase in J_2. For a gap of $\Delta = 10.3$ K, J_2 would be more than 30 times smaller than J_1, which is quite small. For a proper estimation of the magnitudes of the three exchange constants (J_1, J_2 and J_3), we have chosen temperatures corresponding to two values of χ; one at the maximum and the other where χ saturates to its paramagnetic value. The Hamiltonian corresponding to this system can be written as $H = \Sigma_i\{[J + (-1)^{i-1}\delta]S_i\cdot S_{i+1} + J_3S_i\cdot S_{i+2}\}$, where $(J \pm \delta)$ corresponds to J_1 and J_2.[26] We solve this Majumdar−Ghosh Hamiltonian for a range of system sizes (two and three unit cells) with $S = 5/2$ spins and with exchange parameters J_1, J_2 and J_3. We find that the best fit to the experimental data is obtained with $J_2 = J_3 = 0.35J_1$. All three exchange interactions are antiferromagnetic and their magnitudes are also reasonable considering the distance between the corresponding spin centres.[27]

The dependence of magnetisation (M) as a function of magnetic field (B) at 5 and 15 K are shown in Figure 4. For both temperatures $M(B)$ increases rapidly with increasing B, indicating that the excited spin states are significantly populated. It is clear from the figure that at these temperatures there is no alignment of spins. For a comparison, we have computed Brillouin functions for two independent $S = 5/2$ spins in the unit cell and for a large unit cell with $S =$

 © 2004 Wiley-VCH Verlag GmbH & Co. KGaA, Weinheim

5. The $M = f(B)$ curve at $T = 15$ K is between the two Brillouin functions mentioned above. This proves that even at $T = 15$ K, the magnetic polarisation of the unit cell with two high-spin Fe^{3+} ions is not complete. Since the lowest excited spin state is a triplet with a gap of 10 K, the sharp initial rise in $M(B)$ for small B values corresponds to the Zeeman-coupling-assisted increase in population of the triplet state. With the fitted values of the exchange parameters ($J_2 = J_3 = 0.35J_1$), we have computed the magnetisation for the temperature values, $T = 5$, 15 and 30 K. For $T = 15$ and 30 K, they are plotted with the corresponding experimental $M = f(B)$ curves for comparison. In the inset of Figure 3, we have plotted all three theoretical $M = f(B)$ curves up to high magnetic field strengths. The $M = f(B)$ curve at $T = 5$ K closely follows Brillouin functions with one independent $S = 5$ unit-cell spin. Thus, at small T, the magnetisation corresponds to the magnetic polarisation of one unit cell (1 unit cell = 2 Fe^{3+} ions). We estimate theoretically that for the complete alignment of the spins on all the unit cells (complete polarisation) for this one-dimensional ladder would require magnetic field strengths of the order of 8 Tesla even at low temperatures (i.e. about 5 K).

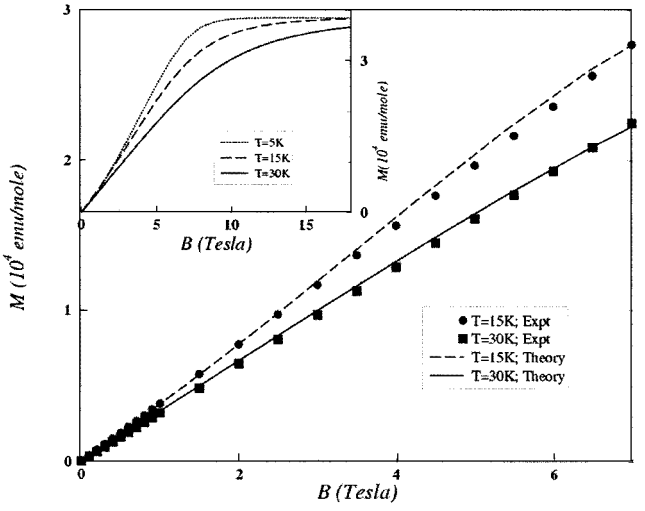

Figure 4. Magnetisation (M) as a function of magnetic field (B) at two different temperatures, $T = 5$ K (filled circles) and $T = 15$ K (filled squares); the dashed line and the solid line are the theoretical magnetisation plots for the corresponding T values; the inset shows the theoretical M vs. B curve for three different temperatures, $T = 5$ K (dotted line), $T = 15$ K (dashed line) and $T = 30$ K (solid line)

Conclusions

The synthesis, structure and magnetic characterization of a one-dimensional iron arsenate, $^1_\infty[NH_3(CH_2)_2NH(CH_2)_2NH_3][Fe_2F_4(HAsO_4)_2]$ (**I**), has been accomplished. The theoretical estimate of the exchange parameters based on the Majumdar−Ghosh model shows the presence of a frustrated solid with one strong and two weak short-range antiferromagnetic couplings. A two-dimensional layer structure built up exclusively from SBU-4 units has been reported recently by us,[28] and we have now stabilized SBU-4 in a one-dimensional structure. More importantly, the low-dimensional structures of the type investigated here provide an opportunity for the theoretical evaluations of the interplay between the coupling strength, the geometrical frustrations and the low-temperature phase transitions, as such materials are rarely isolated. We are vigorously pursuing further work in this direction.

Experimental Section

Compound **I** was synthesized hydrothermally in the presence of diethylenetriamine (DETA). In a typical synthesis iron acetylacetonate [Fe(acac)$_3$] (0.196 g) was dispersed in water (2 mL). To this, As_2O_5 (0.378 g) and HF (48%, 0.08 mL) were added while stirring continuously. Finally, DETA (0.25 mL) was added, and the mixture was homogenised at room temperature for 30 min. The reaction mixture with the composition Fe(acac)$_3$/As_2O_5/HF/DETA/H_2O (1:3:4:4:200) was transferred into a PTFE-lined stainless-steel pressure vessel (23 mL) and heated at 180 °C under autogenous pressure for 72 h. The initial pH of the reaction mixture was approximately equal to 5 and the pH after the reaction was approximately 4. The resulting product, a crop of fine pale-yellow rod-shaped crystals, was filtered, washed with water and dried at room temperature (yield 70% based on Fe). An EDAX analysis indicated that the ratio Fe/As was 1:1, and that fluorine was present. $C_4H_{17}As_2F_4Fe_2N_3O_8$ (572.75): calcd. C 8.4, H 3.0, N 6.3; found C.8.1, H 2.8, N 6.3. A potentiometric titration also confirmed the presence of fluorine (calcd. 13.27%; found 12.9%).[29]

A suitable single crystal was carefully selected under a polarising microscope and glued to a thin glass fibre. Crystal structure determination by X-ray diffraction was performed with a Siemens Smart-CCD diffractometer equipped with a normal focus, 2.4 kW sealed-tube X-ray source (Mo-K_α radiation, $\lambda = 0.71073$Å) op-

Table 2. Crystal data and structure refinement parameters for $^1_\infty[NH_3(CH_2)_2NH(CH_2)_2NH_3][Fe_2F_4(HAsO_4)_2]$ (**I**)

Empirical formula	$C_4H_{17}As_2F_4Fe_2N_3O_8$
Formula mass	572.75
Crystal size [mm]	0.06 × 0.16 × 0.16
Crystal system	triclinic
Space group	$P\bar{1}$ (No. 2)
a [Å]	5.5386(5)
b [Å]	9.5537(9)
c [Å]	13.6893(12)
α [°]	89.780(2)
β [°]	83.799(2)
γ [°]	76.230(2)
V [Å^3]	699.24(11)
Z	2
$D_{calcd.}$ [g·cm^{-3}]	2.720
μ [mm^{-1}]	6.865
Total data collected	2990
Unique data	1992
Observed data [$I > 2\sigma(I)$]	1726
R_{merg}	0.0476
R indexes [$I > 2\sigma(I)$]	$R_1 = 0.0319$[a]; $wR_2 = 0.0687$[b]
R indexes (all data)	$R_1 = 0.0409$[a]; $wR_2 = 0.0738$[b]

[a] $R_1 = ||F_o| - |F_c||/|F_o|$. [b] $wR_2 = \{[w(F_o^2 - F_c^2)^2]/[w(F_o^2)^2]\}^{1/2}$; $w = 1/[\sigma^2(F_o)^2 + (aP)^2 + bP]$, $P = [\max.(F_o^2,0) + 2(F_c)^2]/3$, where $a = 0.0164$ and $b = 2.9953$.

 © 2004 Wiley-VCH Verlag GmbH & Co. KGaA, Weinheim

Table 3. Selected bond lengths [Å] and angles [°] in $^1_\infty[NH_3(CH_2)_2NH(CH_2)_2NH_3][Fe_2F_4(HAsO_4)_2]$ (**I**); values in brackets are the bond valences; their sum SVB appears in bold type at the end of the list of the distances around every cation; symmetry transformations used to generate equivalent atoms: #1: $x-1, y, z$; #2: $-x, -y+1, -z+2$; #3: $x+1, y, z$; #4: $-x+3, -y, -z+3$

Bond		Bond	
As(1)−O(1)	1.669(4) [1.303]	Fe(1)−O(4)#2	1.992(4) [0.533]
As(1)−O(2)	1.678(4) [1.272]	Fe(1)−O(2)	1.999(4) [0.523]
As(1)−O(3)	1.687(4) [1.241]	Fe(1)−F(11)#2	2.024(3) [0.394]
As(1)−O(4)	1.685(4) [1.248]	Fe(1)−F(11)	2.054(3) [0.363]
Σ(As−O)	[5.065]	Σ(Fe−O/F)	[3.014]
As(2)−O(5)	1.679(4) [1.269]	Fe(2)−F(10)	1.913(3) [0.531]
As(2)−O(6)	1.693(4) [1.221]	Fe(2)−O(8)#3	1.941(4) [0.611]
As(2)−O(7)	1.665(4) [1.317]	Fe(2)−O(5)#4	1.978(4) [0.553]
As(2)−O(8)	1.710(4) [1.167]	Fe(2)−F(9)#4	1.982(3) [0.441]
Σ(As−O)	[4.974]	Fe(2)−O(6)	2.008(4) [0.510]
Fe(1)−F(12)	1.874(3) [0.590]	Fe(2)−F(9)	2.064(3) [0.353]
Fe(1)−O(3)#1	1.941(4) [0.611]	Σ(Fe−O/F)	[3.000]
Angle		**Angle**	
O(1)−As(1)−O(2)	110.9(2)	O(2)−Fe(1)−F(11)	83.43(15)
O(1)−As(1)−O(4)	104.77(19)	F(11)#2−Fe(1)−F(11)	78.52(14)
O(2)−As(1)−O(4)	113.64(19)	F(10)−Fe(2)−O(8)#3	92.25(15)
O(1)−As(1)−O(3)	108.5(2)	F(10)−Fe(2)−O(5)#4	90.68(15)
O(2)−As(1)−O(3)	108.97(19)	O(8)#3−Fe(2)−O(5)#4	98.22(17)
O(4)−As(1)−O(3)	109.89(18)	F(10)−Fe(2)−F(9)#4	168.03(14)
O(7)−As(2)−O(5)	110.4(2)	O(8)#3−Fe(2)−F(9)#4	99.71(14)
O(7)−As(2)−O(6)	111.6(2)	O(5)#4−Fe(2)−F(9)#4	87.18(14)
O(5)−As(2)−O(6)	111.06(19)	F(10)−Fe(2)−O(6)	90.65(15)
O(7)−As(2)−O(8)	104.7(2)	O(8)#3−Fe(2)−O(6)	93.82(16)
O(5)−As(2)−O(8)	110.79(18)	O(5)#4−Fe(2)−O(6)	167.82(16)
O(6)−As(2)−O(8)	108.07(18)	F(9)#4−Fe(2)−O(6)	89.02(14)
F(12)−Fe(1)−O(3)#1	90.58(16)	F(10)−Fe(2)−F(9)	89.46(13)
F(12)−Fe(1)−O(4)#2	90.10(15)	O(8)#3−Fe(2)−F(9)	176.36(15)
O(3)#1−Fe(1)−O(4)#2	98.63(16)	O(5)#4−Fe(2)−F(9)	84.96(14)
F(12)−Fe(1)−O(2)	92.72(16)	F(9)#4−Fe(2)−F(9)	78.62(13)
O(3)#1−Fe(1)−O(2)	92.40(16)	O(6)−Fe(2)−F(9)	82.95(14)
O(4)#2−Fe(1)−O(2)	168.59(16)	As(1)−O(2)−Fe(1)	126.4(2)
F(12)−Fe(1)−F(11)#2	171.96(14)	As(1)−O(3)−Fe(1)#3	132.6(2)
O(3)#1−Fe(1)−F(11)#2	97.35(14)	As(1)−O(4)−Fe(1)#2	124.2(2)
O(4)#2−Fe(1)−F(11)#2	87.46(14)	As(2)−O(5)−Fe(2)#4	124.3(2)
O(2)−Fe(1)−F(11)#2	88.24(15)	As(2)−O(6)−Fe(2)	125.3(2)
F(12)−Fe(1)−F(11)	93.66(14)	As(2)−O(8)−Fe(2)#1	132.1(2)
O(3)#1−Fe(1)−F(11)	174.18(15)	Fe(2)#4−F(9)-Fe(2)	101.38(13)
O(4)#2−Fe(1)−F(11)	85.36(14)	Fe(1)#2−F(11)-Fe(1)	101.48(13)

erating at 40 kV and 40 mA. An empirical absorption correction based on symmetry-equivalent reflections was applied with the SADABS program.[30] The structure was solved and refined using the SHELXTL-PLUS suite of programs.[31] All hydrogen atoms were located in the difference Fourier maps. For the final refinement the hydrogen atoms were placed geometrically and held in the riding mode. The final refinement included atomic positions for all atoms, anisotropic thermal parameters for all non-hydrogen atoms and isotropic thermal parameters for all hydrogen atoms. Full-matrix least-squares refinement against $|F^2|$ was carried out using the SHELXTL-PLUS[31] suite of programs. Details of the structure solution and final refinement for $^1_\infty[NH_3(CH_2)_2NH(CH_2)_2NH_3][Fe_2F_4(HAsO_4)_2]$ (**I**) are given in Table 2. CCDC-205336 contains the supplementary crystallographic data for this paper. These data can be obtained free of charge at www.ccdc.cam.ac.uk/conts/retrieving.html [or from the Cambridge Crystallographic Data Centre, 12 Union Road, Cambridge CB2 1EZ, UK; Fax: (internat.) + 44-1223-336-033; E-mail: deposit@ccdc.cam.ac.uk].

Acknowledgments

S. N. thanks the Council of Scientific and Industrial Research, (CSIR) Government of India and S. K. P. thanks the Department of Science and Technology (DST), Government of India for financial support.

[1] F. D. M. Haldane, *Phys. Rev. Lett.* **1983**, *50*, 1153−1156.
[2] W. L. J. Buyers, R. M. Morra, R. L. Armstrong, M. J. Hogan, P. Gerlach, K. Hirakawa, *Phys. Rev. Lett.* **1986**, *56*, 371−374.
[3] S. Ma, C. Broholm, D. H. Reich, B. J. Sternlieb, R. W. Erwin, *Phys. Rev. Lett.* **1992**, *69*, 3571−3574.
[4] D. J. Scalapino, *Nature* **1995**, *377*, 12−13.
[5] E. Dagotto, T. M. Rice, *Science* **1996**, *271*, 618−623.
[6] M. Azuma, Z. Hiroi, M. Takano, K. Ishida, Y. Kataoka, *Phys. Rev. Lett.* **1994**, *73*, 3463−3466.
[7] M. Azuma, Z. Hiroi, M. Takano, Y. Bando, Y. Takeda, *Nature* **1992**, *356*, 775−776.
[8] R. S. Eccleston, T. Barnes, J. Brody, J. W. Johnson, *Phys. Rev. Lett.* **1994**, *73*, 2626−2629.

 © 2004 Wiley-VCH Verlag GmbH & Co. KGaA, Weinheim

[9] G. Chaoussant, P. A. Crowell, L. P. Levy, O. Piovesana, A. Madouri, D. Mailly, *Phys. Rev. B* **1997**, *55*, 3046−3049.
[10] M. Hase, I. Terasaki, K. Uchinokura, *Phys. Rev. Lett.* **1993**, *70*, 3651−3654; M. Nishi, O. Fujita, J. Akimitsu, *Phys. Rev. B* **1994**, *50*, 6508−6510.
[11] A. K. Cheetham, G. Ferey, T. Loiseau, *Angew. Chem. Int. Ed.* **1999**, *38*, 3268−3292 and references therein.
[12] S. Ekambaram, S. Sevov, *Inorg. Chem.* **2000**, *39*, 2405−2410.
[13] P. Feng, T. Zhang, X. Bu, *J. Am. Chem. Soc.* **2001**, *123*, 8608−8609.
[14] A.-H. Liu, S.-L. Wang, *Inorg. Chem.* **1998**, *37*, 3415−3418.
[15] M.-Y. Lee, S.-L. Wang, *Chem. Mater.* **1999**, *11*, 3588−3594.
[16] S. Chakrabarti, S. Natarajan, *Angew. Chem. Int. Ed.* **2002**, *41*, 1224−1226.
[17] K.-H. Lii, Y.-F. Huang, V. Zima, C.-Y. Huang, H.-M. Lin, Y.-C. Jiang, F.-L. Liao, S.-L. Wang, *Chem. Mater.* **1998**, *10*, 2599−2609 and references therein.
[18] Ch. Baerlocher, L. B. McCusker, *Database of Zeolite Structures*: http://www.iza-structure.org/databases/
[19] M. Eddaoudi, D. B. Moler, H. L. Li, B. L. Chen, T. M. Reineke, M. O'Keeffe, O. M. Yaghi, *Acc. Chem. Res.* **2001**, *34*, 319−330.
[20] G. Ferey, *J. Fluorine Chem.* **1995**, *72*, 187−193 and references therein.
[21] M. Riou-Cavellec, D. Riou, G. Ferey, *Inorg. Chim. Acta* **1999**, *291*, 317−325.
[22] G. Ferey, *Chem. Mater.* **2001**, *13*, 3084−3098 and references therein.
[23] I. D. Brown, D. Altermatt, *Acta Crystallogr., Sect. B* **1985**, *41*, 244−247.
[24] M. Troyer, H. Tsunetsugu, D. Wurtz, *Phys. Rev. B* **1994**, *50*, 13515−13527.
[25] D. C. Johnston, R. K. Kremer, M. Troyer, X. Wang, A. Klümper, S. L. Bud'ko, A. F. Panchula, P. C. Canfield, *Phys. Rev. B* **2000**, *61*, 9558−9606.
[26] R. Chitra, S. K. Pati, H. R. Krishnamurthy, D. Sen, S. Ramasesha, *Phys. Rev. B* **1995**, *52*, 6581−6587.
[27] S. K. Pati, S. Ramasesha, D. Sen, *Magnetism: Molecules to Materials IV* (Eds. J. S. Miller, M. Drillon), Wiley-VCH, Weinheim, **2003**, p. 119.
[28] S. Chakrabarty, S. K. Pati, M. Green, S. Natarajan, *Eur. J. Inorg. Chem.* **2003**, 3820−3825.
[29] *Vogel's Textbook of Quantitative Chemical Analysis*, Vth ed., John Wiley & Sons Inc., New York, **1989**. p. 570.
[30] G. M. Sheldrick, *SADABS, Siemens Area Detector Absorption Correction Program*, University of Göttingen, Göttingen, Germany, **1994**.
[31] G. M. Sheldrick, *SHELXTL-PLUS, Program for Crystal Structure Solution and Refinement*, University of Göttingen, Göttingen, Germany, **1997**.

Received February 17, 2004
Early View Article
Published Online July 27, 2004

 © 2004 Wiley-VCH Verlag GmbH & Co. KGaA, Weinheim